Renewable and Sustainable Energy Reviews 16 (2012) 2980–2987

Contents lists available at SciVerse ScienceDirect

Renewable and Sustainable Energy Reviews

journal homepage: www.elsevier.com/locate/rser

Experimental validation of pressure loss in anemometer testing equipment

Michele Messina*

Department of Mechanical and Industrial Engineering, Faculty of Engineering, University of Catania, Catania, Italy

ARTICLE INFO

Article history:
Received 14 June 2011
Received in revised form 8 February 2012
Accepted 10 February 2012
Available online 22 March 2012

Keywords:
Anemometer testing equipment
Energy efficiency
Wind tunnel
Pressure losses

ABSTRACT

This work deals with an experimental procedure to validate theoretical equations used for pressure losses inside anemometer testing equipment. This equipment allows for the generation of air flow inside a chamber designed for anemometer calibration testing at different air speeds. To calibrate anemometers to high accuracy, the air flow must have very low turbulence and uniform velocities over the testing chamber cross section. For high performance, the anemometer testing equipment used a closed-circuit wind tunnel design.

In designing the anemometer testing equipment, the pressure losses of single components were evaluated as well as overall pressure loss utilizing theoretical equations found in the scientific literature. Once the pressure losses were evaluated, the fan was chosen to ensure volumetric flow, balance pressure losses and above all maximise its performance.

With the design completed, the anemometer testing equipment was built, and a campaign of experimental measurements was performed to evaluate the accuracy of the theoretical pressure loss equations. The campaign was performed in two different conditions: closed testing chamber and open testing chamber. The results showed good agreement between the theoretical and experimental pressure losses for the closed testing chamber. Conversely, a discrepancy was revealed for the open condition. The origin of this discrepancy was investigated and a new equation proposed.

Contents

1. Introduction

The anemometer testing equipment is a tool for calibrating anemometers. It provides air flow with known intensity, direction and turbulence levels. The better the air flow quality, the better the anemometer calibration quality. This equipment can be configured in different ways. The simplest and most economical is when it consists of a blower and a contraction. Being the simplest, it produces the poorest air flow quality (high level of turbulence). To improve air flow quality, the anemometer testing equipment must be built as a closed circuit wind tunnel. So, to ensure it is of the highest quality, it must be designed with the same rules adopted for the design of a closed circuit wind tunnel. On the basis of the author's previous experience [1], it was built as a reduced size closed circuit wind tunnel (0.63 m × 2.36 m).

There are many types of wind tunnel and they can be classified by flow speed. They can be divided into four groups:

- subsonic or low speed wind tunnels;
- transonic wind tunnels;

* Corresponding author. Fax: +39 095337994.
E-mail address: mmessina@diim.unict.it

1364-0321/$ – see front matter © 2012 Elsevier Ltd. All rights reserved.
doi:10.1016/j.rser.2012.02.025

- supersonic wind tunnels;
- hypersonic wind tunnels.

Low speed wind tunnels are the most common. Transonic wind tunnels are common in the aircraft industry since most commercial aircraft operate in this regime. Supersonic wind tunnels can be used to investigate the behavior of jet engines and military aircraft. Hypersonic wind tunnels find their applications in rockets and space vehicles.

Moreover, low speed wind tunnels are classified into 'open circuit' or 'closed circuit'. In open circuit wind tunnels, there are no corners or long diffusers but the power needed to drive them is high because of the loss of energy in the out-flowing air. Closed circuit wind tunnels re-circulate the air and thus need less power to achieve a given flow speed and above all, facilitate well-controlled flow conditions in the test section. The anemometer testing equipment described in this paper is of this type (low speed closed-circuit wind tunnel).

Wind tunnel design is a complex field involving numerous fluid mechanics and engineering issues. Some books and articles have been written on this topic [2,3] and are useful references when designing and constructing low speed wind tunnels.

The first enclosed wind tunnels were designed and built in 1870 [4] by Francis Herbert Wenham (a Council Member of the Aeronautical Society of Great Britain), and today scientific research on this topic is still ongoing. In [5], Lindgren and Johansson implemented the concept of expanding corners, producing a compact wind tunnel circuit without compromising flow quality. To decrease the turbulence level, Terashima [6] investigated the use of octahedral blocks. Based on intensive investigation and well-constructed wind tunnels, Hou et al. [7] review some new ideas on low turbulence wind tunnel design. The paper describes a supplementary curve to incorporate in the design of a stable section which plays a crucial role in reducing turbulence intensity. In [8], Li et al. face the problem of noise inside a wind tunnel. The main problems in aero-acoustic wind tunnel design are considered, and their acoustic design methods are pointed out. In [9], Liu et al. explain in detail aerodynamic design, accessory facility design, structure design, construction type, the results of flow field measurement, and the characteristics of a multifunction boundary-layer wind tunnel. This example provides a reference for designing and constructing similar wind tunnels. In [10], Van Pelt et al. designed and built a self-contained portable wind tunnel that is easily transported on a tandem-axle trailer and pulled by a pickup truck. This wind tunnel has been used to test rangeland and cropped surfaces in several locations providing reliable soil erosion and dust emission data. In [11], to investigate the sound from fluid–structure interactions, a low-noise wind tunnel was designed and built. The aerodynamic and acoustic calibration of the tunnel were discussed in relation to design criteria. In [12], Ouyang et al. discuss the design criteria for an open jet wind tunnel that can operate with nozzles of different dimensions. Both the aerodynamic and acoustic design of the wind tunnel's components are discussed in detail. In [13], Winkler and Carolus give an overview of design criteria and specifications, along with an aeroacoustic and aerodynamic characterization of a wind tunnel. In [14], Li and Yang use computational fluid dynamics to simulate flow in an aero-acoustic model wind tunnel. The flow field and pressure losses associated with each piece of the major components are thus found numerically.

This is a brief literature review on wind tunnels, because many other issues today are involved in the scientific research on wind tunnels which is still ongoing so as to reduce wind tunnel dimensions and costs and to maximize performance.

Anemometer testing equipment components are specifically designed and built to ensure the testing chamber has optimum space uniformity and is independent of air flow time.

The overall dimensions of anemometer testing equipment depend mainly on the testing chamber dimensions which once known together with the test type, all the other components can be designed.

To achieve very low turbulence, the anemometer testing equipment used a closed-circuit wind tunnel design with high quality flow and independent of weather conditions and other extraneous activities. It requires less energy compared to the open-circuit wind tunnel and produces less noise. Its testing chamber has a square cross-section (100 mm × 100 mm) with a design average flow velocity of about 30 m/s along its axis. Furthermore, it has two diffusers, three corners (with turning vanes) to guide the flow around the 90° corners, a fan to ensure mass flow rate and balance any pressure loss throughout the circuit, a settling chamber with a honeycomb (to eliminate any transverse flow) and a series of ever-finer mesh screens (to reduce turbulence), a nozzle to accelerate flow and provide constant velocity over the whole testing chamber. The pressure losses of single components were evaluated as well as overall pressure loss. Once the pressure losses were evaluated, the fan was chosen to ensure the design's volumetric flow, balance pressure losses and above all maximise its performance. At the end of the design process, on-design and off-design performance were evaluated to obtain the equipment's characteristics in a defined velocity range (0–30 m/s).

Once designed, the equipment was built, and the effective pressure losses were measured with a calibrated hot wire and a differential manometer. The experimental measurements were performed in two different testing chamber operating conditions: open and closed. The measurements showed good agreement with theoretical equations for the closed testing chamber, while there was an appreciable discrepancy for the open testing chamber.

2. Anemometer testing equipment design and build

The anemometer testing equipment is a complete and compact system which allows for an air flow to be generated inside ducts designed for anemometer calibration testing at different air speeds.

To achieve very low turbulence, the equipment uses a closed-circuit wind tunnel design. Its main components are shown in Fig. 1.

The first step in wind tunnel design is defining a priori the testing chamber criteria which are dimensions, shape and desired air velocity. Here, a square testing chamber with a 0.1 m side was used with an air velocity of 30 m/s.

The testing chamber length has to be in the range of 0.5–3 times its hydraulic diameter [2]. This choice takes into account that the airflow exiting the nozzle needs 0.5 times the hydraulic diameter to become almost uniform. Moreover, a long testing chamber (more than 3 times the equivalent hydraulic diameter) could increase boundary layer thickness causing the boundary layer to detach at the testing chamber exit.

So, in this equipment the length of the testing chamber was set to twice the hydraulic diameter of the testing section.

Moreover, to avoid air velocity reduction and an increase in boundary layer thickness at the sharp edges of the testing chamber, the sharp edges should be rounded off. 45° chamfers are best.

The contraction or 'nozzle' accelerates the flow from the settling chamber to the testing section, further reducing any variations in velocity.

In a wind tunnel, the nozzle is the most difficult component to design. Flow velocity and its uniformity within the testing chamber cross-section depend on the nozzle's design. The nozzle exit cross-section dimensions and shape are identical to the testing chamber

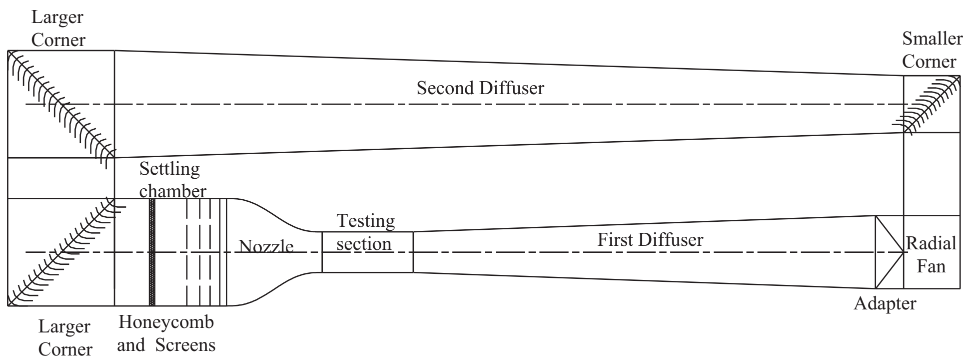


Fig. 1. Anemometer testing equipment.

ones since they are joined together. Consequently, the nozzle also has 45° chamfers.

Knowing the nozzle exit cross-section dimensions and shape, those of its inlet cross-section must be determined.

The nozzle area ratio should be 'as large as possible', to reduce the total-pressure loss through the screens mounted between the settling chamber and the nozzle (see Fig. 1). Normally, the nozzle inlet/outlet cross-section area ratio should be in the range of 6–10 [17]. Area ratios greater than 10 lead to excessive inlet dimensions while area ratios less than 6 lead to high pressure loss through the screens.

For the anemometer testing equipment, an area ratio of 7 was chosen. With the inlet and outlet nozzle cross-sections, the nozzle's silhouette is defined by fifth order Bell–Metha polynomials [17] represented mathematically by Eq. (1).

$$y = \sum_{i=0}^{5} a_i x^i \tag{1}$$

where x is the axial direction inside the nozzle, and y represents the half side length of the local section of the nozzle.

A nozzle should have the ratio "axial length"/"side length of inlet cross-section" (L/l'), about equal to 1 [17].

In fact, it was experimentally evident that a L/l' ratio less than 0.667 causes the air flow to detach close to the nozzle exit, whilst a value greater than 1.79 increases boundary layer thickness.

For this equipment, the value of L/l' was set to 0.91, obtaining a nozzle length of 0.254 m.

In order to design the second diffuser, the inlet cross-section area must first be calculated while the exit is equal to the nozzle inlet cross-section area. The second diffuser inlet cross-section area is governed by the fan dimensions (see Fig. 1).

Therefore, it is essential to first design the fan.

To evaluate the outlet section of the fan, from the specialist literature [17], it is known that the ratio between the fan cross-section area A_f and the testing chamber cross-section area A_{ts} has to be in the range of 2–3.

To use an A_f/A_{ts} ratio value greater than 3 is not recommended because irregular flow velocities at the fan entrance may be generated. To use an A_f/A_{ts} ratio value less than 2 is also not recommended because it may increase the overall wind tunnel dimensions (higher wind tunnel construction costs).

An A_f/A_{ts} ratio equal to 2 is a good choice for maintaining low wind tunnel dimensions and costs. For the anemometer testing equipment an A_f/A_{ts} ratio equal to 2 was used.

The usual design rule for subsonic diffusers is that the total included angle ($2\vartheta_e$) of a portion of a circular cone with the same length (L) and area ratio (A_R) as the diffuser should not exceed a maximum value ($2\vartheta_e\big|_{\max} = 6^\circ$ [2]).

With the hydraulic diameters of the inlet and outlet diffuser cross-sections, the equivalent cone expansion angle can be calculated given by Eq. (2).

$$\vartheta_e = \arctan\left(\frac{1}{2}\,\frac{\sqrt{A_R}-1}{L/D_{h1}}\right) \tag{2}$$

D_{h1} is the inlet section's hydraulic diameter. For this equipment, $2\vartheta_e = 4^\circ$ was chosen.

Solving Eq. (2) for L, the minimum diffuser length can be determined (1.956 m for this test case).

The first diffuser inlet cross-section area and shape are known because they equal the cross-section area and shape of the testing chamber. The outlet cross-section area depends on the inlet area of the fan.

This wind tunnel is a closed-loop type so flow must be deflected by 90° three times with minimum turbulence at the three corners. For this reason the corners are equipped with bent flat plates.

The smaller corner has a square cross-section equal to the fan outlet's. The bent flat plates' leading edges are set to 5°, while the trailing edges are 0°. Thus, the bent flat plates' chord is calculated for 85°.

Adjacent to the second larger corner there is a settling chamber with a constant cross-sectional area. The aim of a settling chamber which contains honeycombs and screens is to reduce flow turbulence before it enters the nozzle.

The settling chamber cross-sectional area matches the dimensions of the other components it is attached to, while the settling chamber length is designed to fit the gap between the components close to the wind tunnel loop.

In this case, the total settling chamber length is 0.261 m and is able to contain one honeycomb and three screens. The honeycomb with its cells aligned in the flow direction is able to reduce fluctuating variations in transverse velocity [21]. The honeycomb has little effect on stream-wise velocity due to the fact that the pressure drop through a honeycomb is small [21].

In the honeycomb design procedure, its length (L_h), cell hydraulic diameter (D_h), and porosity (β_h) are key factors [15].

Honeycomb porosity is defined as the ratio of actual cross-section area flow over the total cross-section area.

Two main criteria have to be verified in wind tunnel honeycomb design. These criteria are expressed by Eqs. (3) and (4) [15].

$$6 \le \frac{L_h}{D_h} \le 8 \tag{3}$$

$$\beta_h \ge 0.8 \tag{4}$$

To establish if the chosen honeycomb meets the test-case wind tunnel design, the two criteria expressed by Eqs. (3) and (4) have to be verified.

Table 1
Component pressure loss at $c_{ts} = 30$ m/s (c_{ts}, testing section air speed).

Components	Δp (Pa)
Closed testing section	16.4
First diffuser	54.6
Adapter	1.0
Constant-area section	2.9
Smaller corner	26.3
Second diffuser	16.1
Larger corner	2.5
Constant-area section	0.07
Larger corner	2.5
Settling chamber	0.18
Honeycomb	4.5
First screen	10.5
Second screen	11.1
Third screen	11.9
Nozzle	2.1
Total pressure loss	162.8

It is well known that screens mainly reduce stream-wise velocity fluctuations, with little effect on flow direction [21]. Moreover, it has been demonstrated [21] that a series of screens with different mesh qualities (coarse, medium and fine) is more efficient than only one fine mesh screen.

To effectively reduce turbulence, screen porosity must be in the range of 0.58–0.8 [15].

$$0.58 \le \beta_s \le 0.8 \tag{5}$$

Screen porosity values over 0.8 are not suitable for good turbulence control, while values below 0.58 lead to flow instability.

2.1. Pressure losses

Closed-loop wind tunnel pressure loss is calculated by considering wind tunnel sections separately.

In a wind tunnel, pressure losses occur as consecutive pressure losses in different sections. Overall pressure loss ($\Delta p_{overall}$) equals the pressure gain due to the fan.

In wind tunnel component i, pressure loss (Δp_i) can be written as the product of constant K_i and the dynamic pressure at the entrance of the component (see Eq. (6)).

$$\Delta p_i = K_i \times \frac{1}{2}\rho_i c_i^2 \tag{6}$$

where c_i is the mean flow velocity (in the section) at the entrance of component i.

Wind tunnel screens are installed to control turbulence just before the nozzle inlet. Eckert [16] proposes an empirical relation for the screen loss coefficient based on three main parameters: porosity or its complement solidity, the Reynolds number calculated with wire diameter Re_w, and mesh factor K_{mesh}. The latter was studied by I.E. Idel'chik [19] who assigned it a value of 1.0 for new metallic wires, 1.3 for circular metallic wires, and 2.1 for silk fibres. An average value of 1.3 for K_{mesh} is a good choice in most cases.

To determine pressure loss in honeycombs, the three main parameters of stream-wise length to cell hydraulic diameter ratio, porosity and Reynolds number based on cell hydraulic diameter must be accounted for Eckert et al. [16]. Nozzle pressure loss is only considered as due to skin friction.

Since nozzle pressure loss is about 3% of total loss, errors evaluating K_{nt} are less significant than those made in the high-velocity wind tunnel sections, as proposed by Wattendorf [18].

With the above criteria, the loss coefficients for each wind tunnel component can be calculated. Table 1 shows pressure drops for each wind tunnel component.

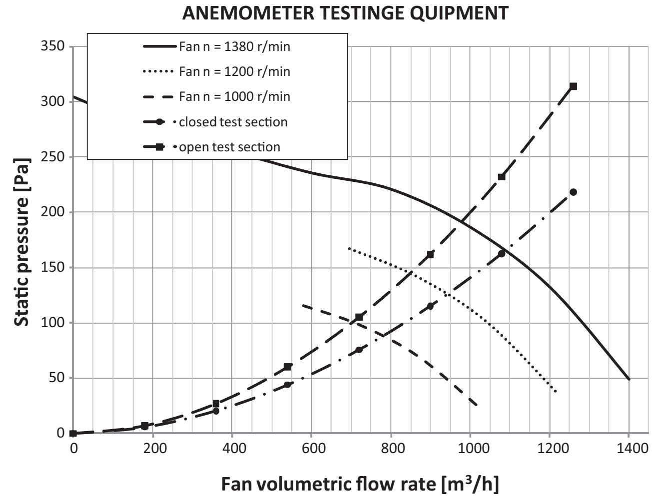


Fig. 2. Fan-anemometer testing equipment matching.

Summing all the wind tunnel section pressure drop values produces total pressure drop (in this case total pressure drop equalled 162.80 Pa) which has to be compensated for by the wind tunnel fan.

2.2. Fan choice

Fans generate air motion within the anemometer testing equipment. The design process consists essentially of choosing a fan from the manufacturer's catalogue and matching it to the equipment. The first step is determining the mechanical characteristics of the anemometer testing equipment (overall pressure drop as a function of air velocity in the testing section). The air velocity in the testing section can also be expressed as a function of the fan's volumetric flow rate using the mass conservation equation. Two different mechanical characteristics can be calculated: one for the closed testing section and another for the open testing section.

The two curves above can be superimposed onto the mechanical characteristics of the fans (supplied by the fan manufacturer) with matching points graphically determined. The best match indicates the most suitable fan.

In Fig. 2 there are three curves for the fan at three different rotation speeds, and two anemometer testing equipment curves for closed and open testing sections, respectively named 'closed testing section' and 'open testing section'. The closed testing section curve shows the pressure drop in all the anemometer testing equipment components as a function of the fan's volumetric flow rate, for the closed testing chamber case; the open testing section curve shows the pressure drop in all the anemometer testing equipment components as a function of the fan's volumetric flow rate for the open testing chamber case.

By applying this matching procedure, a 230 W radial fan at 1380 rev/min was chosen.

Fig. 2 shows the intersection points at three different fan rotation speeds. At the maximum fan rotation speed ($n = 1380$ rev/min) the matching points give 1080 m^3/h and 30.3 m/s in the testing section (closed testing chamber case) and 975 m^3/h and 27.1 m/s in the open testing chamber case.

From 0 to 1380 rev/min, testing section air velocities from 0 to 0.3 m/s are achievable in the closed configuration and from 0 to 27.1 m/s in the open configuration.

3. Pressure losses: experimental validation

3.1. Experimental setup

To evaluate the static pressure drop inside the anemometer testing equipment (see Fig. 3), the testing section was equipped

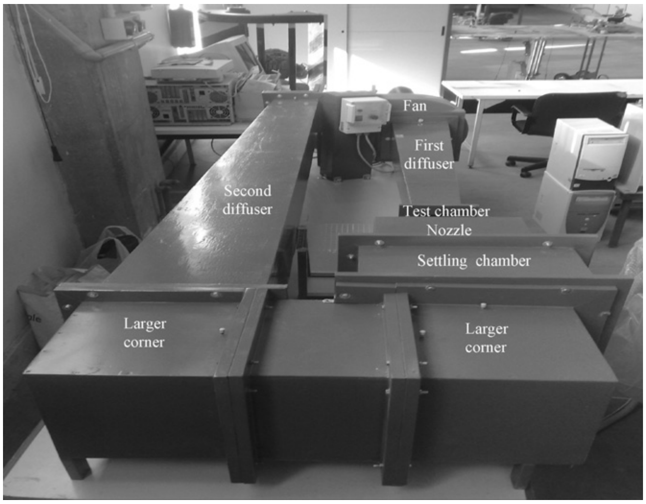


Fig. 3. View of the anemometer testing equipment.

with a calibrated hot wire anemometer and a thermometer (see Figs. 4 and 5), the fan with a differential manometer and a controller to vary its rotation velocity, and the outlet cross section of the nozzle with a static pressure sensor.

The hot wire anemometer measures the air velocity inside the testing chamber at different fan rotation velocities. The differential manometer reads the pressure at nozzle exit while the temperature sensor inside the thermo-anemometer reads the temperature inside the testing chamber. The pressure and temperature inside the testing chamber have to be measured to correctly compare the pressure drop inside the anemometer testing equipment with the fan's curves furnished by the manufacturer and evaluated at the reference pressure and temperature. The differential manometer mounted at the inlet and outlet of the radial fan measures the pressure drop across the fan at different fan rotation velocities. This pressure drop coincides with the pressure drop in the anemometer testing equipment. The fan balances the pressure losses inside the anemometer testing equipment.

3.2. Experimental measurements

Pressure losses were evaluated for air streams inside the testing chamber from 0 to 30 m/s for the closed testing chamber configuration and from 0 to 20 m/s for the open one.

Fig. 6 shows a comparison of the theoretical and experimental pressure losses for the closed testing chamber configuration. The comparison shows good agreement.

In the open testing chamber configuration this does not happen (see Fig. 7).

To theoretically evaluate pressure loss in the anemometer testing equipment, it was evaluated in all the equipment's components. For the open testing chamber, Eqs. (6) and (7) were applied.

For a constant-area section, pressure loss in the testing section (Δp_{ts}) along the duct is proportional to its length (L_{ts}), hydraulic

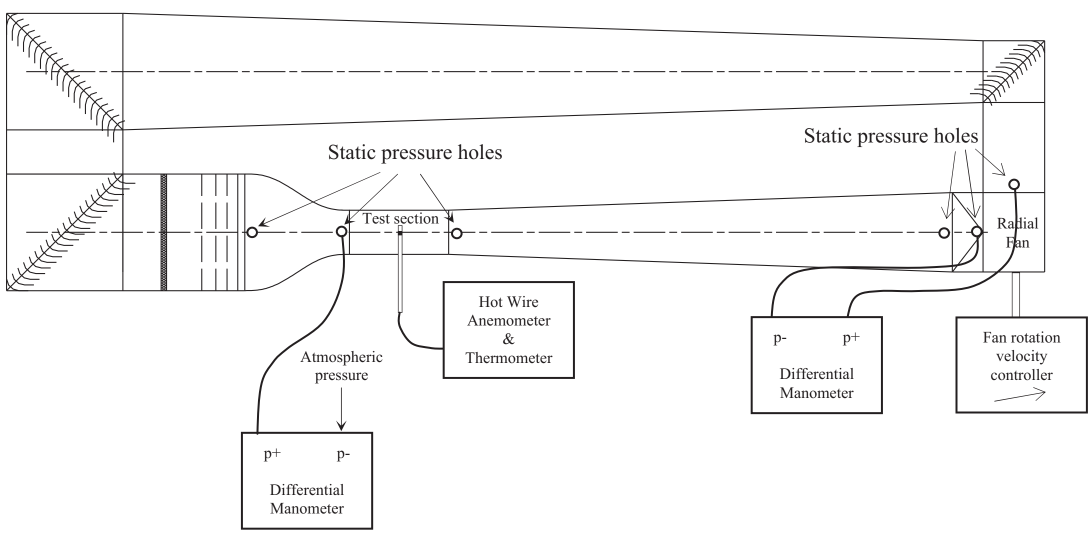


Fig. 4. Experimental setup.

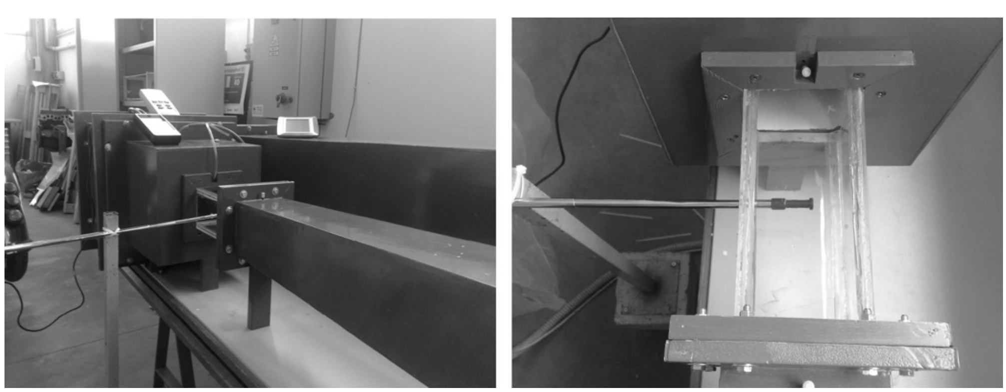


Fig. 5. Instrumented anemometer testing equipment (left); closed testing chamber with hot wire anemometer (right).

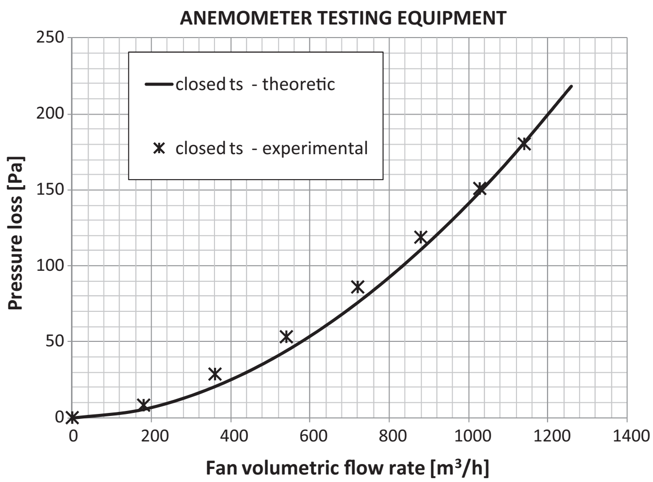


Fig. 6. Overall pressure losses inside the equipment (closed testing chamber).

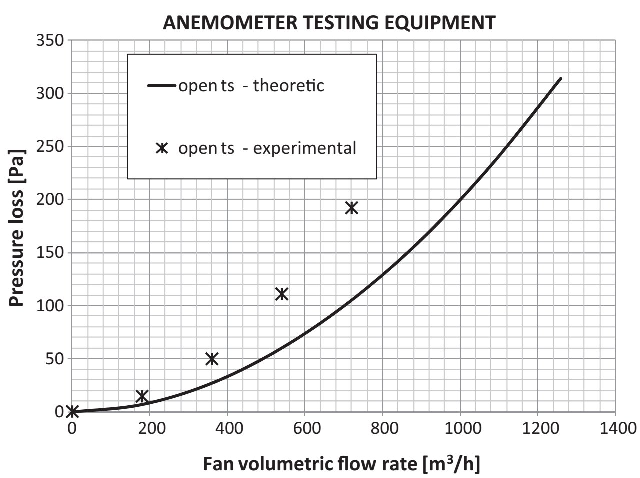


Fig. 7. Overall pressure losses inside the equipment (open testing chamber).

diameter (D_{h-ts}), fluid density (ρ), friction factor (f_{ts}), and the square of mean flow velocity (c_{ts}).

$$K_{ts} = f_{ts}\frac{L_{ts}}{D_{h-ts}} \tag{7}$$

For a closed testing section, for smooth pipes at high Reynolds numbers, Shames [20] uses the Prandtl universal law of friction to determine the friction factor:

$$f_{ts}\big|_{i+1} = [2\log_{10}(Re\sqrt{f_{ts}\big|_i}) - 0.8]^2 \tag{8}$$

where

$$Re = \frac{\rho c_{ts} D_{h-ts}}{\mu} \tag{9}$$

Eq. (8) can easily be solved iteratively from a tentatively chosen friction factor value. A starting value as distant as $f_{ts} = 1$ will lead to convergence within four to six iterations.

For an open testing chamber, a reasonable friction factor is $f_{ts} = 0.08$ [2].

This is true when the air jet leaving the nozzle is perfectly aligned with the testing chamber and the first diffuser. In reality this never happens.

Moreover, with increasing distance from the nozzle, the air jet's cross section increases as it comes into contact with the first diffuser flange (see Fig. 8) which acts as a perpendicular barrier to the motion of the air increasing the pressure loss.

Due to air jet misalignment, it is also possible to have vortices and recirculation on one side of the first diffuser inlet. These vortices and recirculation increase the pressure loss (see Fig. 8).

$f_{ts} = 0.08$ is the minimum ideal value for the friction factor.

In reality, f_{ts} will be greater than 0.08. By increasing the alignment of the air jet with the axis of the testing chamber, and by decreasing the distance between nozzle and diffuser the f_{ts} value will decrease.

To correctly evaluate the friction factor, it was necessary to measure the real pressure loss across the testing chamber. By varying the rotation velocity of the fan, pressure drop was measured by a differential manometer linked to two static pressure holes at the testing chamber inlet and outlet (see Fig. 4). The real pressure losses in the open testing chamber provide the correct value for the friction factor $f_{ts} = 0.23$ (see Fig. 9).

Taking into account the real pressure drop inside the testing chamber ($f_{ts} = 0.23$), it is possible to correctly evaluate the pressure losses inside the anemometer testing equipment (see Fig. 10).

Once the pressure losses through the anemometer testing equipment in both open and closed testing chamber configurations have been evaluated, the fan's characteristic curve can be matched to those of the anemometer testing equipment (see Fig. 11).

The curve intersections in Fig. 11 show the theoretical air velocity in the testing chamber (open and closed).

Table 2 shows the theoretical and experimental air velocity in the testing chamber.

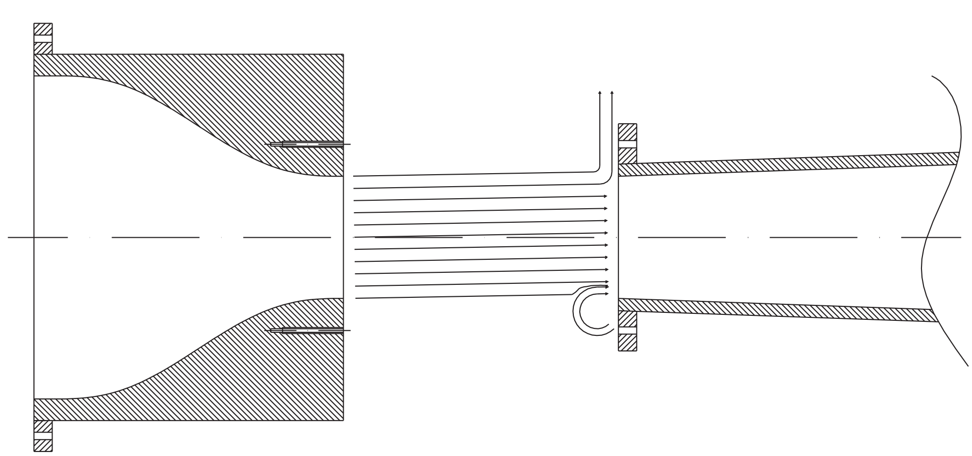


Fig. 8. Misalignment of the air jet leaving the nozzle.

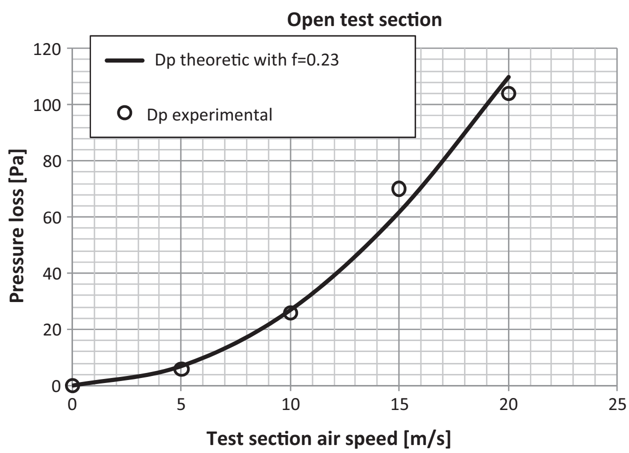


Fig. 9. Pressure loss in the open testing chamber.

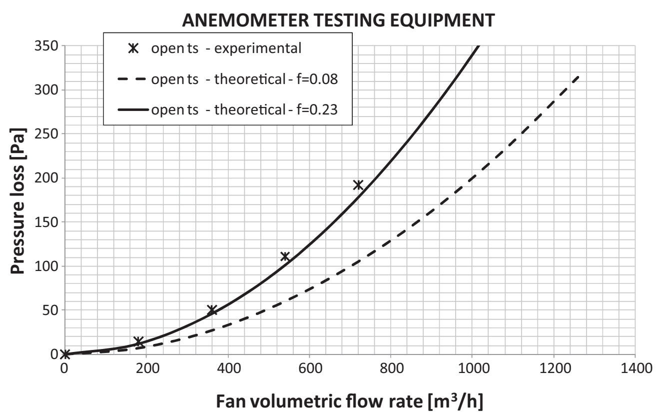


Fig. 10. Pressure loss in the anemometer testing equipment (open testing chamber).

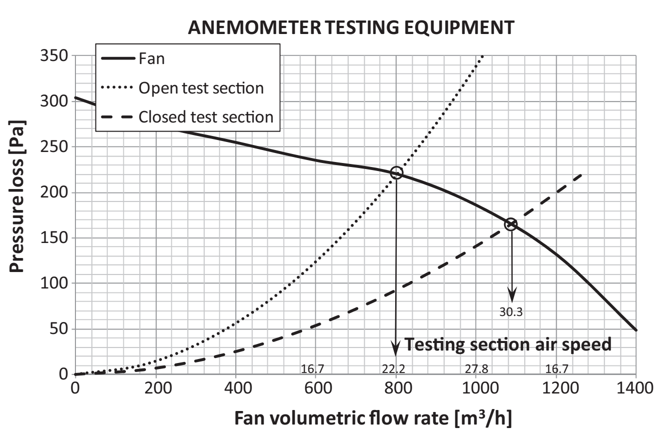


Fig. 11. Fan-anemometer testing equipment matching.

Table 2
Theoretical and experimental air velocity in the testing chamber.

	c_{ts} – theoretical (m/s) (Fig. 11)	c_{ts} – experimental (m/s)
Open testing section	22.2	21.7
Closed testing section	30.3	30.8

The data in Table 2 show good agreement between the experimental and theoretical evaluation based upon the new friction factor.

In conclusion, during the design of anemometer testing equipment with the geometry of a closed circuit wind tunnel, the theoretical equation found in scientific literature for the evaluation of pressure loss can be implemented safely, except for pressure loss in the open configuration where it is vital to significantly increase the friction factor reported in [2].

3.3. Future developments for anemometer testing equipment

In the settling chamber, the honeycomb reduces the transverse component of the airflow and increases airflow alignment with the testing chamber axis. Alignment accuracy is related to honeycomb cell size (9 mm) and the honeycomb's axial length (62 mm). With this geometry the alignment accuracy is $\pm 4.15^{\circ}$.

In the future, to improve air jet alignment with the testing chamber axis, a new second larger corner will be designed and built.

The new corner will present swinging turning vanes to further reduce the misalignment, reduce pressure loss, and permit greater air velocity.

4. Conclusion

This work presents an experimental procedure for validating theoretical equations for evaluating pressure loss inside anemometer testing equipment.

The anemometer testing equipment used a closed circuit wind tunnel design, to maximize air jet quality inside the testing chamber and reduce noise when the equipment is running. Once defined, the design specifications (testing chamber dimension and air flow velocity within), and pressure loss were evaluated and the fan chosen.

Post design, the anemometer testing equipment was built, and a campaign of experimental measurements was performed to evaluate the worth of the theoretical pressure loss equations.

The campaign of experimental measurements was performed in two different conditions: closed testing chamber and open testing chamber. The campaign of experimental measurements showed good agreement between theoretical and experimental pressure loss for the closed testing chamber condition. Conversely, in the open testing chamber condition a discrepancy was found whose origin is due to a misalignment of the air jet within it. Due to such a misalignment, vortices and recirculation on one side of the entrance of the first diffuser may be generated, increasing pressure loss.

Moreover, the greater the distance from the nozzle, the greater the air jet cross-section at the first diffuser flange which acts as a perpendicular barrier to air motion also increasing pressure loss.

After a set of pressure loss experimental measurements across the open testing chamber, a correction in the friction factor in the theoretical equation was proposed.

References

[1] Brusca S, Lanzafame R, Messina M. Low-speed wind tunnel: design and build. In: Pereira JD, editor. Wind tunnels: aerodynamics, models and experiments. New York: Nova Science Publishers, Inc.; 2011., ISBN 978-1-61209-204-1 p. 189–220.
[2] Barlow JB, Rae WH, Pope A. Low-speed wind tunnel testing. 3rd ed. John Wiley & Sons; 1999.
[3] Bradshaw P, Pankhurst RC. The design of low-speed wind tunnels. Progress in Aeronautical Sciences 1964;6(1–69).
[4] Dodson MG. An historical and applied aerodynamic study of the Wright Brothers' wind tunnel test program and application to successful manned flight. US Naval Academy. Report USNA-1531-2; 2005.

[5] Lindgren B, Johansson AV. Evaluation of a new wind tunnel with expanding corners. Experiments in Fluids 2004;36:197–203, doi:10.1007/s00348-003-0705-y.
[6] Terashima O. The proper design of rectifying device for the wind tunnel. Journal of Wind Engineering 2011;36(2):23–7.
[7] Hou ZY, Wang LZ, Zhou JH, He KM. The further research on the design of low (varying) turbulence wind tunnel. Journal of Experiments in Fluid Mechanics 2011;25(1):92–6.
[8] Li P, Tang GS, Yu YS, Lü B. Research of acoustic design for aeroacoustic wind tunnel. Journal of Experiments in Fluid Mechanics 2011;25(3):82–6.
[9] Liu QK. Aerodynamic and structure design of multifunction boundary-layer wind tunnel. Journal of Experiments in Fluid Mechanics 2011;25(3):66–70.
[10] Van Pelt RS, Zobeck TM, Baddock MC, Cox JJ. Design, construction, and calibration of a portable boundary layer wind tunnel for field use. Transactions of the ASABE 2010;53(5):1413–22.
[11] Ouyang H, Zhu Y, Tian J, Du Z. Design and characterization of a small aeroacoustic wind tunnel. Noise Control Engineering Journal 2010;58(1.):67–73.
[12] Sarradj E, Fritzsche C, Geyer T, Giesler J. Acoustic and aerodynamic design and characterization of a small-scale aeroacoustic wind tunnel. Applied Acoustics 2009;70(8):1073–80.
[13] Winkler J, Carolus T. Concept, design and characterization of a small aeroacoustic wind tunnel facility with application to airfoil measurements. Noise Control Engineering Journal 2009;57(4):370–83.
[14] Li QL, Yang ZG. Application of CFD for the design of aero-acoustic wind tunnel. Acta Aerodynamica Sinica 2009;27(3):373–7.
[15] Metha RD, Bradshaw P. Design rules for small low speed wind tunnels. Journal of Royal Aeronautical Society 1979;73.
[16] Eckert W, Mort KW, Pope J. Aerodynamic design guidelines and computer program for estimation of subsonic wind tunnel performance. Washington, DC: National Aeronautics and Space Administration. NASA TN D-8243; October 1976.
[17] Bell JH, Metha RD. Contraction design for small low-speed wind tunnels. NASA-CR-182747; April 1988.
[18] Wattendorf FL. Factors influencing the energy ratio of return flow wind tunnels. In: Fifth international Congress for applied mechanics. 1938.
[19] Idel'chick IE. Handbook of hydraulic resistance. The Israel Program for Scientific Translation, Tel Aviv, AEC-TR-6630; 1966.
[20] Shames IH. Mechanics of fluids. 3rd ed. New York: McGraw Hill; 1992.
[21] Prandtl L. Attaining a steady stream in wind tunnel. NACA TM 726; October 1933.